RSC Advances

PAPER

View Article Online
View Journal | View Issue

Cite this: *RSC Adv.*, 2017, **7**, 4921

Magnetic paper – based ELISA for IgM-dengue detection†

G. A. Ortega,[ab] S. Pérez-Rodríguez[c] and E. Reguera*[a]

Received 28th October 2016
Accepted 20th December 2016

DOI: 10.1039/c6ra25992h

www.rsc.org/advances

This contribution reports a novel "Magnetic Paper – Based ELISA" using core–shell magnetite@polydopamine nanoparticles supported on a Whatman paper-like new solid immunoassay platform specifically for IgM-dengue antibodies recognition as the proof-of-concept target for antibodies isotype IgM detection. Affordable procedures to deposit magnetite nanoparticles on cellulose paper sheets (Whatman type-1 and ss903) and to conjugate such nanoparticles with anti human-IgM antibodies using polydopamine as linker are reported. Structural features, magnetic behavior, coating homogeneity, and the nanoparticles/linked antibodies ratio were determined. Additionally, "Magnetic Paper – Based ELISA" for IgM-dengue antibodies detection provides a system with improved analytical response (two orders more sensitive with a 700 times lower limit of detection (LOD) than traditional ELISA or using magnetic beads without depositing), appropriate accuracy for real sample detection, low cost, easy manufacturing, and effortless and easy handling.

Introduction

Nowadays, the most used methodology for antigens detection (*e.g.*, enzymes, proteins, antibodies, and nucleic acids) is the enzyme linked immunosorbent assay known as ELISA, which was introduced by Engvall and Perlmann in 1971.[1] Besides, in recent years new variants of ELISA as well as blot and western blot assays with novel solid supports have been widely used. In this sense, magnetic beads and nanoparticles, mainly magnetite, are even patented (US20140212990A1) and commercialized as a new platform.[2–4] Magnetite nanoparticles (Fe_3O_4) provide a solid support with greater surface area, thus increasing the conjugated biomolecules amount and avidity, and resulting in improved analytical sensor performance.[5] In addition, washing protocols can be automated with magnets.

The most common studies are based on a sandwich assay supported on magnetite micro-beads and superparamagnetic nanoparticles in: (i) colloidal suspension,[6] (ii) conventional[7] and printed electrodes,[8,9] (iii) thin-film transistor,[10] (iv) microfluidic system,[11] and (v) automatic portable[12] and screening[13,14] devices for separation and detection[15] of proteins (enzymes, antibodies mainly type IgG),[16] nucleic acid,[17] virus,[18,19] bacteria,[20] and cancer biomarkers.[21]

The above mentioned devices do not only employ conventional detection systems such as optical,[22] fluorescent,[23] or electrochemical,[24] but also new technologies have been introduced for analytical responses based on magnetic[25–28] and optical[29–31] properties of new supports.

However, most of these technologies can be costly and impractical for the diagnosis of certain endemic and epidemic diseases in underdeveloped countries, where a considerable amount of patient samples must be studied.

On the other hand, the most important application of paper (cellulose material) support of sensors by the scientific community in recent years has been the development of new paper-based analytical devices (PAD) including paper-based colorimetric[32] and electrochemical[33,34] ELISA. This technique has advantages and disadvantages in terms of sensitivity, simplicity, and cost-effectiveness. Paper, or cellulose in general, is attractive for sensing applications for several reasons: (i) paper is a low-cost, easily available, biodegradable, and lightweight material; (ii) cellulose fibers can be functionalized; (iii) the microfiber network morphology increases the surface to volume ratio and loading capacity; (iv) its porous structure and hydrophilic character results in remarkable wetting, permeability, and reactivity properties, giving rise to lateral and capillary-driven flows and hydrophilicity. However, for paper-

[a]*Center for Applied Science and Advanced Technology of IPN, Legaria Unit, Mexico City, Mexico. E-mail: edilso.reguera@gmail.com*

[b]*University of Havana, Faculty of Chemistry, Department of Inorganic Chemistry, Havana, Cuba*

[c]*National Autonomous University of Mexico, Biomedical Research Institute, Mexico City, Mexico*

† Electronic supplementary information (ESI) available: XRD powder patterns of Fe_3O_4 and Fe_3O_4@PDA nanoparticles; TEM micrographs of PDA nanoparticles; ATR-FT-IR spectrum of Fe_3O_4, Fe_3O_4@PDA and the different capped papers; TGA analysis of different paper samples; mass magnetization *versus* applied magnetic field and ZFC/FC curves for Fe_3O_4 and Fe_3O_4@PDA powders and supported on paper W1; SDS-PAGE technique and Bradford assay analysis and data information; synthesis and characterization of AgNP-based SERS nanoparticles; microscopic images for capped papers; study of different blockers for magnetite PDA coated papers; titration in estimating the effective amount of Fe_3O_4@PDA-AntiIgM for capture as many IgM-dengue and quantitative detection of IgM-dengue spiked in human serum samples by magnetic paper – based ELISA method with Fe_3O_4@W1-PDA as solid support. See DOI: 10.1039/c6ra25992h

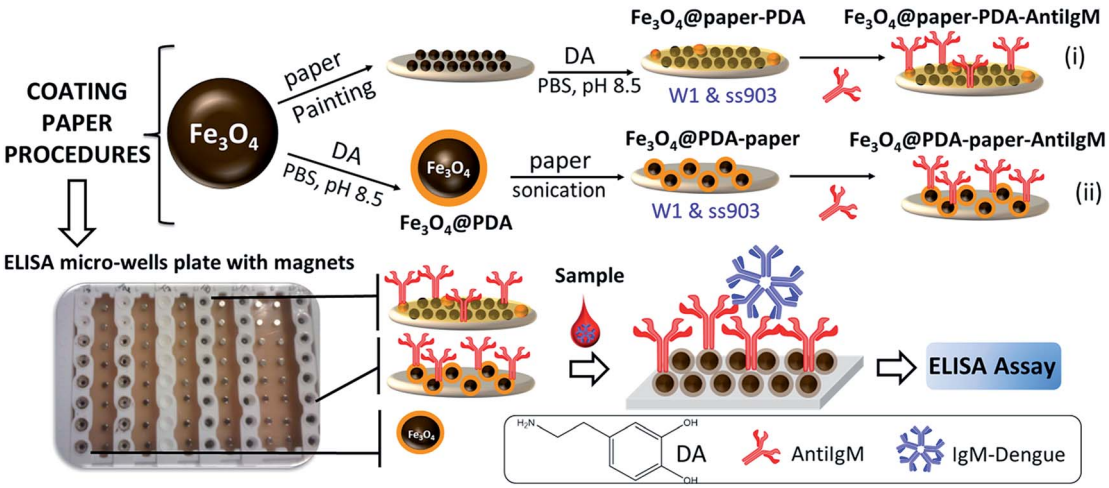

Scheme 1 Representation of the procedures for coating papers and conjugated with anti-human IgM antibodies.

based ELISA assay the sensitivity is currently more than ten times lower than that of traditional ELISA[35] due to high background associated with unspecific biomolecules adsorption.

Furthermore, to our knowledge there is a relative lack of reports on magnetic-ELISA or, generally speaking, nanoparticles-based immunoassays for sensing antibodies isotype IgM. Probably, the huge IgM molecular weight makes it difficult for coupling efficiency plus steric hindrance adversely affects recognizing capability. However, numerous traditional IgM antibodies-capture ELISA (MAC-ELISA) are designed for diagnosis of illnesses which have primary specific IgM antibody responses such as for the dengue virus.

In this work, two ways of coating paper (Whatman type-1 (W1; commonly reported in paper-biosensor devices) and ss903 (commonly used in blood sample collection cards)) were explored (see Scheme 1):

(i) By first coating papers with Fe_3O_4 nanoparticles, later growing polydopamine shell (PDA) on the Fe_3O_4-paper surface (Fe_3O_4@paper-PDA), and finally coupling AntiIgM antibodies (Fe_3O_4@paper-PDA-AntiIgM);

(ii) By using core–shell Fe_3O_4@PDA nanoparticles previously synthesized and then deposited on a paper surface (Fe_3O_4@-PDA-paper) on which AntiIgM antibodies are immobilized (Fe_3O_4@PDA-paper-AntiIgM).

The synergy between the advantages of components provides a versatile product. The effects of different parameters like structural features, magnetic behavior, coating homogeneity, and the nanoparticles/linked antibodies ratio were explored. As far as we know, this is the first attempt to develop "Magnetic Paper – Based ELISA" as a new solid immunoassay platform specifically for IgM-dengue antibodies recognition as a proof-of-concept target for antibodies isotype IgM.

Materials and methods

Materials

All reagents were purchased from Sigma-Aldrich. The antibody anti-human IgM (μ-chain specific) produced in rabbits, were purchased from Sigma-Aldrich cod. SAB3701409. UMELISA DENGUE IgM PLUS kit was obtained from Immunoassay Center, Cuba. Used healthy human serum samples were obtained from the authors of this work with our consent, and were also analyzed with standard confirmatory procedures for dengue detection (IgM-ELISA, NS_1-ELISA, and PCR) to confirm absence of the illness. Real samples of infected patients were not analyzed.

Methods

Synthesis of magnetite nanoparticles. Fe_3O_4 nanoparticles were prepared by a chemical coprecipitation method. $FeCl_3$ (3.24 g) was dissolved in 200 mL of 1.2 mM HCl by ultrasound treatment under a N_2 atmosphere. Afterward, $FeSO_4 \cdot 7H_2O$ (2.78 g) was added by vigorous stirring. Then, 1.25 M aqueous NaOH solution (300 mL) (previously deoxygenated) was added dropwise under vigorous stirring (100 drops per minute), forming a black Fe_3O_4 precipitate. After vigorous stirring for another 30 min, the precipitate was magnetically decanted and washed thoroughly with ultrapure water until the supernatant solution reached neutrality (pH = 7).

Synthesis of magnetite nanoparticles functionalized with polydopamine (PDA). For coating with PDA, 200 mg of Fe_3O_4 were dispersed under continuous stirring and ultrasound treatment in 10 mL of 3 mg mL^{-1} of dopamine solution in PBS, (pH = 8.5) at room temperature, overnight. After that, polydopamine modified nanoparticles (Fe_3O_4@PDA) were magnetically decanted, washed thoroughly with ultrapure water to remove the non-reacted dopamine, and further dispersed in 10 mL of water.

Deposition of core–shell Fe_3O_4@PDA on paper and conjugated with anti-human IgM antibodies (AntiIgM)

Two ways for coating paper with Fe_3O_4@PDA and functionalized with AntiIgM were studied:

Fe_3O_4@W1-PDA-AntiIgM and Fe_3O_4@ss903-PDA-AntiIgM. (1) Deposition of Fe_3O_4 nanoparticles on paper Whatman-type 1

(W1) and Whatman-type ss903 (ss903): (Fe_3O_4@W1 and Fe_3O_4@ss903).

3 mL (57 mg mL^{-1}) of Fe_3O_4 dispersion was spread over aluminium paper. Then, paper W1 (circle diameter of 90 mm) or ss903 (circle diameter of 10 mm) according to the case, were immersed into the "magnetic ink" and covered with another piece of aluminium paper. Then, the sandwich was rolled with a "rolling pin" to homogenize the magnetite on paper. After that, the magnetite coated papers were kept in horizontal arrangement during drying under N_2 flow to avoid a gradient of concentration along the paper.

(2) Coating Fe_3O_4@W1 and Fe_3O_4@ss903 with PDA.

Fe_3O_4@W1 and Fe_3O_4@ss903 were submerged in 3 mg mL^{-1} of dopamine solution in PBS, (pH = 8.5) under stirring at room temperature overnight. The reaction was stopped by washing (three times) in a deionized water pool.

(3) Circular fragments of paper (Fe_3O_4@paper-PDA and Fe_3O_4@PDA-paper), with diameters of 5 mm made with a paper punching machine, were deposited in pristine microwells with ninety-six-well plates coupled to a magnet for washing steps. Afterward, 0.02 mL anti-human IgM (1 mg mL^{-1}) in PBS (pH = 7.4) was dispensed and incubated for 3 hours at 37 °C and kept at 4 °C overnight. After magnetically decanting and washing (4 times) thoroughly with 0.03 mL of washing solution (tampon Tris–NaCl–Tween 20) to remove non-reacted anti human-IgM, the pieces of paper were treated with blocking buffer (dry milk 5% in PBS pH = 7.4) for 4 h at 37 °C, washed as described above, and stored at 4 °C.

Fe_3O_4@PDA-W1-AntiIgM and Fe_3O_4@PDA-ss903-AntiIgM. 2 mL (45 mg mL^{-1}) of Fe_3O_4@PDA were sonicated for 5 minutes. Then, paper W1 or ss903 (circle diameters of 20 mm) were introduced into the viscous suspension and then continued under sonication for another 15 minutes. Also, the slices of Fe_3O_4@PDA-W1 and Fe_3O_4@PDA-ss903 were dried under a N_2 flow. For coupling AntiIgM antibodies step 3 was followed.

Characterization

The magnetite nanoparticle size distribution, morphologies, and polydopamine shell thickness of coated nanoparticles were analyzed by high resolution transmission electron microscopy (HRTEM JEM-2100), with an accelerating voltage of 200 kV. The covered papers with magnetite were studied using Scanning Electron Microscopy (SEM JSM 7800-JEOL) working at 15.0 kV with a LED detector. X-ray diffraction (XRD) patterns of Fe_3O_4 and Fe_3O_4@PDA were recorded on a D8 Advance (from Bruker) X-ray diffractometer with a rotating anode X-ray generator using 10 to 90°/2θ and Cu Kα radiation (40 kV, 20 mA).

Different systems were characterized using Fourier Transform Infrared spectroscopy (PerkinElmer spectrometer Frontier coupled to an Attenuated Total Reflectance (ATR) accessory). Thermogravimetric (TG) analyses were performed with High Resolution TGA Q5000 IR equipment at heating rates of 10 °C min^{-1} under a continuous nitrogen flow. The magnetic behavior of Fe_3O_4, Fe_3O_4@PDA, and magnetite nanoparticles on a paper surface was investigated by superconducting interference device magnetometry with MPMS (Quantum Design). Zero-field-cooled (ZFC) and field-cooled (FC) magnetizations were recorded as a function of temperature in the presence of 50 Oe field after cooling the sample in the absence (ZFC) or in the presence (FC) of the same probe field.

The amounts of anti-human IgM and IgM-dengue conjugated on Fe_3O_4@PDA were analyzed by Bradford assay and SDS gel electrophoresis. For Bradford assay, a reference solution was prepared with exactly the initial antibody concentration and media conditions (pH, ionic strength) and BSA was used as a protein standard (successive dilutions 1 : 2 from 0.5 mg mL^{-1}). SDS gel electrophoresis was performed as described by Laemmli using a 12.5% polyacrylamide gel (SDS-PAGE) and detection by staining with Coomassie blue.[38]

The homogeneity of Fe_3O_4@PDA-AntiIgM deposited on a paper surface was studied using Raman spectroscopy. Different regions of coating paper surface were scanned with a Thermo Scientific DXR Raman Microscope. During these measurements, a 20× objective (N/A 0.25) and a solid-state laser at 532 nm (1.0 mW) as the excitation source were used for mapping different spots on the surfaces (2 s of exposure time and 20 scans for each recorded spectrum). Fluorescence spectra were recorded on an Edinburgh FS5 spectrofluorometer.

ELISA for IgM-dengue detection

Traditional methodology. Ninety-six-well microtiter plates were coated with 0.02 mL anti-human IgM (1 mg mL^{-1}) in coating buffer (pH 9.6) at 4 °C overnight and treated with blocking buffer (dry milk 5% in PBS pH = 7.4) for 2 h at 37 °C. Afterward, negative and positive controls of IgM-dengue (0.02 mL, 4.5 mg mL^{-1}) were captured by anti-μ chain specific IgM antibodies anchored onto microplates. Then, unlinked components were eliminated by washing; 0.01 mL of four serotypes dengue-specific antigens solutions was added to be captured by IgM-dengue antibodies. Once unlinked antigens were removed, 0.01 mL of biotinylated anti-dengue antigens monoclonal antibodies solution was added. After another washing step, 0.01 mL of streptavidin-alkaline phosphatase conjugated was added to establish whether immunological chains had taken place. The immune-complex was then revealed by adding 0.02 mL of 4-methylumbeliferil phosphate solution. After 10 min of incubation, 0.01 mL of hydrolysed substrate was removed from the plate and diluted in 2.5 mL of PBS 1× (pH = 7.4). The fluorescence spectra were measured in a spectrofluorometer with the excitation maximum at 360 nm and emission maximum at 450 nm.

A calibration curve was measured to determine analytical performance. Different concentrations of IgM-dengue were employed and followed as described in the above protocol.

"Magnetic-ELISA" on Fe_3O_4@PDA colloidal suspension. 40 mg of Fe_3O_4@PDA was dispersed in 1 mg mL^{-1} anti-human IgM solution (1 mL, PBS pH = 7.4) for 3 hours under agitation at 37 °C and kept at 4 °C overnight. The Fe_3O_4@PDA-AntiIgM dispersion were magnetically decanted and washed (4 times) thoroughly with 1 mL of washing solution (tampon Tris–NaCl–Tween 20) to remove the non-reacted anti human-IgM, and then

re-dispersed in PBS (pH = 7.4) at 10 mg mL^{-1} and kept at 4 °C until use.

Different aliquots of Fe_3O_4@PDA-AntiIgM (10 mg mL^{-1}) corresponding to 0.1, 0.3, 0.5, and 1 mg of magnetic core were dispensed in pristine microwells. A ninety-six-well plate was coupled to a magnet for washing steps. Afterward, Fe_3O_4@PDA-AntiIgM was magnetically decanted and 0.02 mL of blocking solution (dry milk 5% in PBS pH = 7.4) was added for 4 h at 37 °C to avoid unspecific proteins adsorption on magnetite nanoparticles. Subsequent steps are the same described for traditional methodology.

"Magnetic paper-based ELISA" blocking study. 5 mm of different magnetite-PDA coated papers (Fe_3O_4@W1-PDA, Fe_3O_4@ss903-PDA, Fe_3O_4@PDA-W1, Fe_3O_4@PDA-ss903) and pristine papers (W1 and ss903) were treated with traditional blockers in PBS (pH = 7.4): BSA (3%), bovine serum (20%) and milk (5%) for 4 hours at 37 °C. After a washing step, streptavidin-alkaline phosphatase (S-AP) was added and incubated for 30 minutes. Also, the systems without blockers were treated with S-AP for 30 minutes and 4 hours, respectively.

"Magnetic paper-based ELISA" on Fe_3O_4@paper-PDA-AntiIgM and Fe_3O_4@PDA-paper-AntiIgM. Depending on the number of samples to be processed, functionalized paper sheets of Fe_3O_4@paper-PDA-AntiIgM and Fe_3O_4@PDA-paper-AntiIgM (with W1 and ss903 papers) were sliced with a paper punch. Circular fragments (5 mm in diameter) were used as the solid support for the ELISA assay described above and magnets were used for the washing steps. The hydrolysed substrate was removed from the plate's microwells containing nanoparticle-paper used as ELISA substrate.

"Magnetic paper-based ELISA" using Fe_3O_4@W1-PDA as solid support. Blocked Fe_3O_4@W1-PDA-AntiIgM pieces of paper (5 mm diameter) were incubated with different concentrations of IgM-dengue antibodies solution (from 0 to 100 μg mL^{-1}) in PBS (pH = 7.4) and compared with a standard assay and 0.1 mg of Fe_3O_4@PDA nanoparticles. For recovery analysis, 5 μL of healthy serum sample was diluted in 100 μL of bovine serum solution and spiked with IgM-dengue concentrations from 0 to 1 μg mL^{-1}. This range of concentration corresponds with results of the calibration curve.

Results and discussion

Characterization of Fe_3O_4 nanoparticles, Fe_3O_4@PDA nanoparticles, and core–shell Fe_3O_4@PDA deposited on paper

Fe_3O_4 nanoparticles were synthesized by coprecipitation of Fe^{2+}/Fe^{3+} ions in alkali media and then capped with polydopamine film through the spontaneous oxygen-mediated self-polymerization of dopamine (DA) in PBS (pH 8.5).

Under reported conditions the PDA in magnetite dispersion gradually changed from colorless to yellow and pink, which endorsed the deposition processes. However, during dopamine polymerization on magnetite coated paper it is also worth noting the black precipitation at the bottom of the vessel, suggesting two competitive processes: PDA aggregation in solution and PDA deposition on substrate.

TEM micrographs showed magnetite nanoparticles with pseudo spherical shapes and average diameter of 10 ± 2 nm (Fig. 1a). For core–shell Fe_3O_4@PDA the analysis revealed that Fe_3O_4 nanoparticles were efficiently coated with a polymeric material of thickness 2.2 ± 0.7 nm (Fig. 1b). Polydopamine aggregates were not observed in TEM images.

XRD pattern peaks can be indexed into a spinel cubic structure (fcc) according to the crystalline nature of Fe_3O_4 (JCPDS 87-0245) with a lattice parameter of 0.8391 nm, which is practically coincident with the reported parameter in the literature (0.8396 nm) for the magnetite phase. The presence of broad peaks indicated the ultrafine nature and small crystallite size of the nanoparticles, which was calculated through the Debye–Scherrer equation by using the full-width at half maximum (FWHM) value of the (311) plane, which results in 13 nm crystals. A similar XRD pattern was observed for core–shell Fe_3O_4@PDA nanoparticles, suggesting that the crystalline structure of the nanomaterial was not affected by coating with the polymer film. On the other hand, an amorphous component was observed at lower pattern angles due to polymer contribution (see ESI, Fig. S1†).

For coated paper with Fe_3O_4, SEM micrographs showed that cellulose paper was covered by agglomerates of nanoparticles surrounding each of them (Fig. 2a and b). Also, during the polydopamine polymerization on magnetite-paper systems by using strategy (i) (see Scheme 1), the PDA deposition on magnetite was followed by an agglomeration-deposition process. SEM images (Fig. 2c and d) revealed PDA nanoparticles covering the magnetite-paper surfaces. Such nanoparticles have spherical shapes, with tendency to form aggregates each other and with an individual average of 81 ± 11 nm diameter, according to TEM image (see ESI, Fig. S2†).

For core–shell Fe_3O_4@PDA synthesis, the ratio between magnetite nanoparticles and dopamine amount results in an elevated deposition rate of the PDA on magnetic substrate, whereas the aggregation rate in solution might retain a relatively low level. On the other hand, in PDA deposition on magnetite-paper composites, the further increase in the dopamine/substrate rate dramatically reduces dopamine mean free path, which substantially accelerates the aggregation rate in solution against the deposition rate on substrate.

According to SEM images, another interesting observation is that cellulose fibers of paper type ss903 have random orientation and larger pore-channels than paper W1. Besides, magnetite deposition and PDA aggregates were obtained as the W1 paper (Fig. 2e and f).

In the case of strategy (ii) for Fe_3O_4@PDA-paper systems (see Scheme 1), aggregates of core–shell Fe_3O_4@PDA deposited on paper surfaces (similar to Fe_3O_4@W1 and Fe_3O_4@ss903 according to the case) were also observed.

ATR-FT-IR spectra of Fe_3O_4, Fe_3O_4@PDA and Fe_3O_4@PDA on paper showed a main band at 537 cm^{-1} assigned to the Fe–O stretching mode from the magnetite phase. This value is different from the signal assigned to the same stretching mode obtained in Fourier transform infrared spectroscopy (FT-IR) in KBr pellets which is reported around 570 cm^{-1}. Actually, generally all the bands are redshifted with regard to those

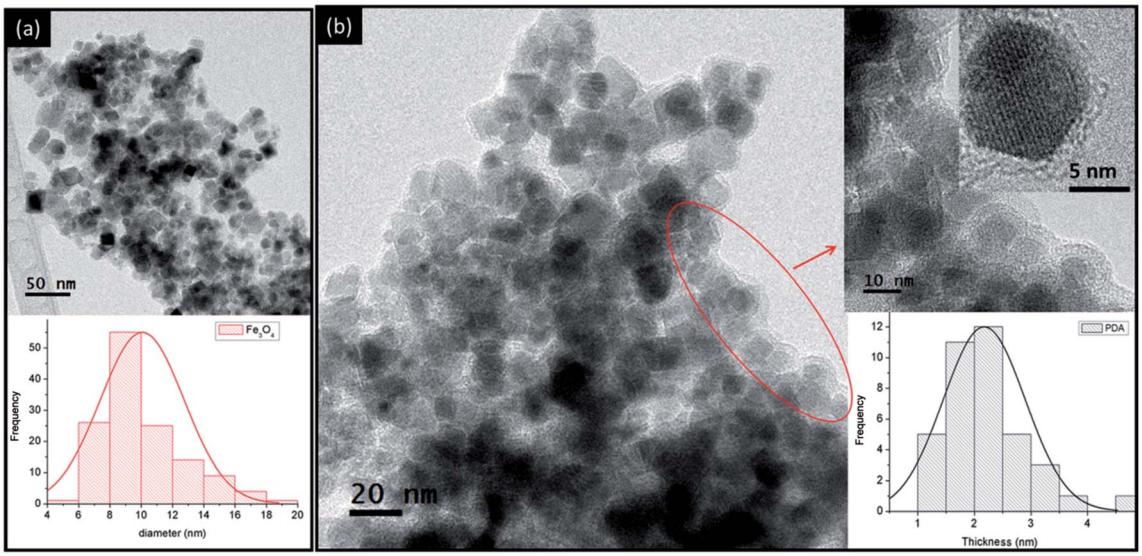

Fig. 1 TEM micrographs of (a) magnetite nanoparticles with size distribution at the bottom and (b) core–shell Fe_3O_4@PDA nanoparticles with thickness distribution at the bottom.

obtained in the KBr pattern. In ATR-FT-IR, parameters such as wavelength of the incident IR radiation, refractive index of the crystal and the sample, light dispersion, and the separation between the crystal and sample could slightly modulate the measured spectrum.

For the core–shell Fe_3O_4@PDA, additional bands in the range of 1600–1482 cm^{-1} ($\nu_{C=C}$, aromatic of polydopamine), 1256 cm^{-1} (ν_{C-N}), 1027 (ν_{C-O}), and 801 cm^{-1} (γ_{C-H}, aromatic of polydopamine or γ_{N-H}) were obtained. In addition, the different capped paper samples: Fe_3O_4@W1-PDA, Fe_3O_4@ss903-PDA, Fe_3O_4@PDA-W1, and Fe_3O_4@PDA-ss903 showed characteristic bands corresponding to the Fe–O stretching mode of magnetite, aromatic stretching mode of polydopamine shell, and an intensive band associated with ν_{C-O} of cellulose (see ESI, Fig. S3†).

Thermal stability of the investigated samples and the amount of magnetite nanoparticles on paper were determined using TGA analysis (see ESI, Fig. S4†). Residue after the thermal degradation of coated paper allowed determining the mass of magnetite contained in the different papers (see ESI, Table S1†). In that sense, the amount of magnetite for Fe_3O_4@W1-PDA, Fe_3O_4@ss903-PDA, Fe_3O_4@PDA-W1, and Fe_3O_4@PDA-ss903 were 0.13, 0.35, 0.25, and 0.17 mg, respectively. Another interesting result is that the decomposition temperature of organic PDA covering magnetite was considerably lower than that for the black precipitate of PDA aggregates. Also, the values for the decomposition temperature of pristine papers are slightly higher than that for papers covered with magnetite. In all cases, the iron oxide performs as a catalyst leading to paper thermal decomposition processes which encourages mandatory incineration after its use in a biological assay.

The magnetic responses as a function of applied magnetic field at 5 K and 300 K, both as powder and supported on paper W1 of pristine magnetite nanoparticles and capping with polydopamine, were recorded (see ESI, Fig. S5a†). Table 1 summarizes the relevant magnetic properties for the samples under study.

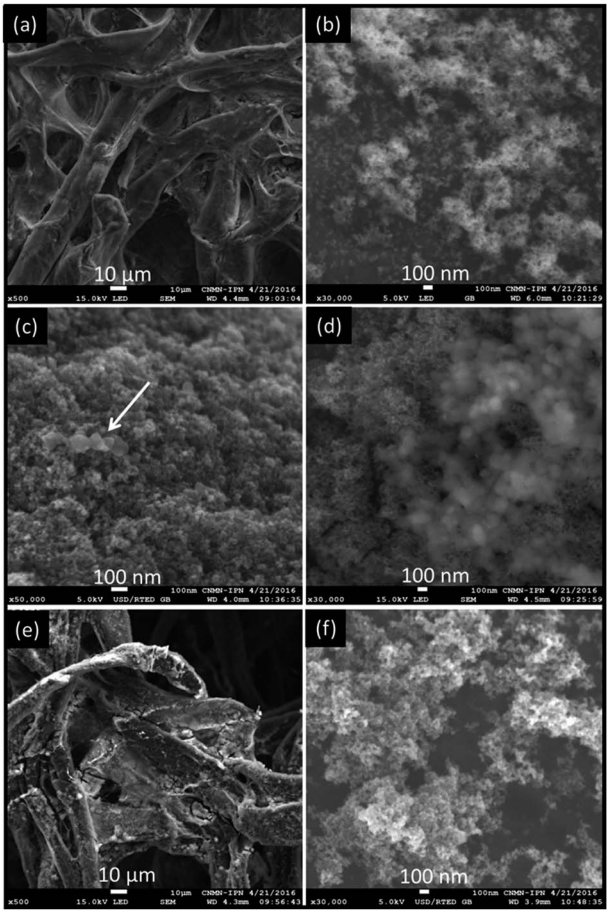

Fig. 2 SEM micrographs of (a and b) Fe_3O_4@W1, (c and d) Fe_3O_4@W1-PDA, (e and f) Fe_3O_4@ss903.

Table 1 Relevant magnetic properties of samples[a]

	M_s* (emu g^{-1})		M_r* (emu g^{-1})		H_c (Oe)		χ_i (emu gOe^{-1})
	5 K	300 K	5 K	300 K	5 K	300 K	300 K
Fe_3O_4	81.3	72.7	19.1	2.8	259	22.4	0.100
Fe_3O_4@PDA	68.0	59.7	15.5	2.8	302	24.6	0.080
Fe_3O_4@W1	2.7	2.11	0.6	0.1	329	25.3	0.003
Fe_3O_4@W1-PDA	11.3	9.7	2.8	0.47	347	25.3	0.015

[a] *Determined with organic content correction in accordance with TGA analysis.

At room temperature, Fe_3O_4 nanoparticles exhibited superparamagnetic behavior with magnetic saturation 72 emu g^{-1}, lower than the bulk magnetite value of 90 emu g^{-1}. In this case, the saturation magnetization can be affected by several features and the magnetostatic interaction responsible for the agglomeration of magnetite particles.

On the other hand, core–shell Fe_3O_4@PDA presents lower saturation magnetization than pristine magnetite nanoparticles, probably due to the surface spin disorder layer. An interesting result is that the aforementioned magnitude for Fe_3O_4@W1-PDA is noticeably higher than the uncovered one. The surfaces of pristine magnetite nanoparticles scattered on the paper are likely susceptible to oxidation during time in atmospheric conditions, leading to the saturation magnetization decrease. Nevertheless, the polydopamine covering shields the magnetite-paper surface by acting as an oxygen scavenger.

The almost immeasurable coercivity (H_c) and remanence (M_r) at room temperature indicate that the samples behave as a superparamagnetic single domain of individual nanoparticles. The initial linear behavior of the magnetization when the external magnetic field is increased from zero was used to calculate the initial magnetic susceptibility (χ_i). This magnitude reflects the effective anisotropy barrier of a material. A larger χ_i value indicates particles that more easily interact magnetically. Comparing their relative χ_i values reveals that a greater level of interparticle interactions occurs between the pristine magnetite nanoparticles relative to others.[36] The behavior of ZFC/FC curves (see ESI, Fig. S5b†) at reported conditions for all samples indicate magnetic interactions and a blocking temperature near to 300 K. For pristine magnetite nanoparticles, TEM images reinforce this assumption; the nanoparticles tend to agglomerate in the absence of a capping agent, provoking the onset of magnetic interactions. For core–shell Fe_3O_4@PDA supported on papers, which are a concentrated granular system, the existing phenomenon could be explained by taking in account that the magnetic clusters are connected with each other, forming macroscopic ensembles with dipolar interaction following ferrimagnetic behaviors. Extrapolation of the linear part in the graph of the FC inverse susceptibility χ^{-1} *versus* temperature, in accordance to the Curie–Weiss law, gives negative values of the ordering Curie temperature for all samples. This suggests a transition from antiferromagnetic to ferrimagnetic order.

According to the magnetic behavior result, for practical purposes for which the system was designed, the most important issue is to guarantee the magnetic response for washing-separation protocols allowing the handling of multiple samples at the same time. In addition, analysis of the magnetic behavior of the magnetite-paper system could be useful for future studies in developing other biosensors based on a superconducting quantum interference device (SQUID), giant magneto resistive sensor chip, or magnetic resonance detection.

Antibodies conjugation

One of the most effective and versatile strategies for biomolecules-nanoparticles coupling is the reaction *via* Schiff bases formation and/or Michael addition adducts of biomolecules amino groups and quinone groups on polydopamine modified surfaces.[37–41]

Furthermore, the amount of antibodies conjugated on nanoparticle surfaces is critical for their recognition capability. In this case, the amount of AntiIgM (IgG isotype antibody) and IgM-dengue antibodies conjugated on core–shell Fe_3O_4@PDA nanoparticles and coated papers surfaces were determined by combining the reductive SDS-PAGE technique and Bradford assay (see ESI S6 for analysis details and Table S2 for data information†).

For AntiIgM antibodies, the difference between the amount determined by using the Bradford method and that obtained through the SDS-PAGE technique corresponds to the amount of antibodies covalently linked to nanoparticle surfaces. For IgM-dengue quantification, the total amount of such antibodies on magnetite-paper systems is able to be determined.

According to the Bradford method, coated paper type ss903 systems exhibit a higher amount of AntiIgM antibodies conjugated, and hence IgM-dengue, than W1. Additionally, the suspension of 1 mg of Fe_3O_4@PDA nanoparticles presents the highest amount of conjugated antibodies. The total coupling yield of AntiIgM per milligram of Fe_3O_4 core functionalized with PDA in suspension or deposited on papers W1 and ss903 was 100%, of which more than 90% of antibodies were covalently linked. According to the SDS-PAGE technique, an important observation is the non-negligible unspecific interaction between antibodies and magnetite coated ss903 papers. In the case of IgM-dengue, the order in the coupling efficiency (per

milligram of magnetite) by means of the prevailing contribution of antigen–antibody interaction was: Fe_3O_4@PDA-ss903 > Fe_3O_4@W1-PDA > Fe_3O_4@ss903-PDA > Fe_3O_4@PDA-W1 ~ Fe_3O_4@PDA (Nps). The above results are a combination of several factors: the higher paper surface area with larger pore-channels and fewer amounts of magnetite-PDA per area, which allows its suitable dispersion and a higher system capability for antibodies coupling.

One of the most important issues which might affect biosensor analytical performance is the homogeneity of conjugated specific receptors for antigen capture (in our case Anti-IgM) on the substrates (nanoparticles-paper surface). The homogeneity of AntiIgM capping magnetite-paper systems (Fe_3O_4@paper-PDA-AntiIgM and Fe_3O_4@PDA-paper-AntiIgM, papers type W1 and ss903) was determined by mapping the surfaces with Raman spectroscopy. However, magnetite nanoparticles are very sensitive to high Raman power lasers due to partial oxidation. Moreover, the Raman spectrum of AntiIgM antibodies is not sufficiently noteworthy to allow its detection.

On the other hand, the highly sensitive Surface Enhanced Raman Scattering (SERS) by using metal nanoparticles, encourages its broad utilization in biomolecule recognition.

In that sense, silver nanoparticles (26 ± 12 nm diameter) were synthesized by using the Turkevich method. A Raman tag (5,5′-dithio-bis(2-nitro-benzoic acid), DTNB) was associated to AgNP surfaces providing strong Raman signals enhanced through SERS phenomenon, while the attached AntiIgM allows specific recognition of IgM-dengue (AgNP-DTNB-AntiIgM) (see ESI S7 for synthesis and characterization details†). Different paper systems functionalized with AntiIgM were incubated with IgM-dengue antibodies under described conditions in the Method section (BSA was used as negative control). After that, AgNP-DTNB-AntiIgM was added to be captured for IgM-dengue immobilized on magnetite-paper surfaces.

Similar intensity values of spectra collected in different spots on the surface suggest homogenous disposition of IgM-dengue and hence AntiIgM on the substrate. Fig. 3 shows Raman spectra for Fe_3O_4@W1-PDA-AntiIgM-IgM and Fe_3O_4@ss903-PDA-AntiIgM-IgM after being incubated with AgNP-DTNB-AntiIgM. According to the recorded spectra, Fe_3O_4@W1-PDA-AntiIgM presents similar Raman signals for different test spots and low background, suggesting favorable homogeneity of the antibodies covering the surface. As SEM micrographs and the images of microscope-coupled Raman spectrometer showed (see ESI, Fig. S8†), magnetite and polydopamine nanoparticles are spread on well coated Fe_3O_4@W1-PDA surfaces leading to the desired result. On the other hand, the analogous system with paper type-ss903 exhibited quite different spectra recovered in several spots, thus confirming non-homogenous covering.

As the SEM image showed, paper type-ss903 has wide and random cellulose channels leading to uncontrolled magnetite deposition and unspecific proteins retention as confirmed by SDS-PAGE. For the system Fe_3O_4@PDA-paper-AntiIgM-IgM, the results were similar to the one obtained for Fe_3O_4@ss903-PDA-AntiIgM-IgM.

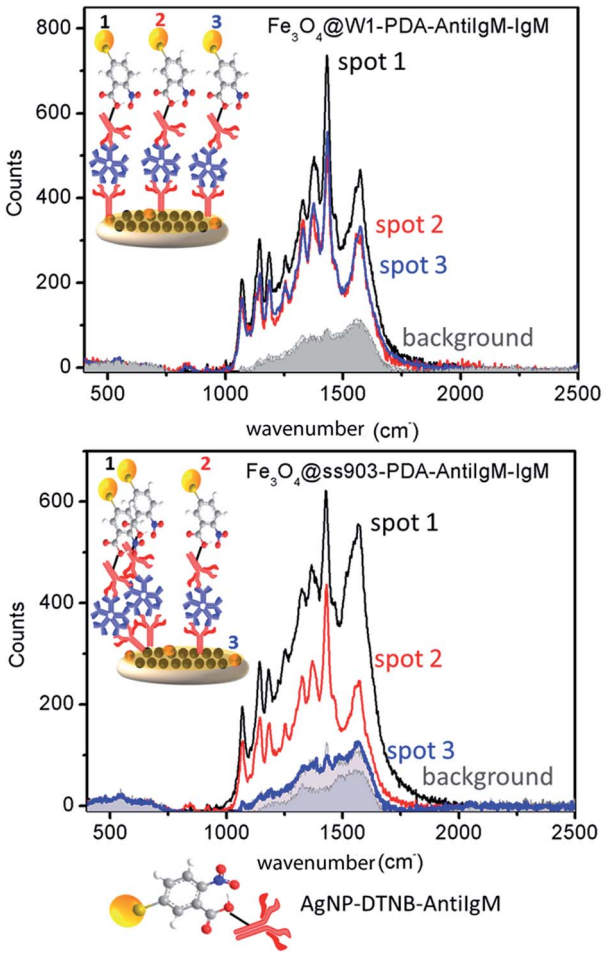

Fig. 3 Raman spectra measured in three different spots on Fe_3O_4@-paper-PDA-AntiIgM-IgM for (at the top) W1 and (at the bottom) ss903 (gray areas are negative controls).

In this case, as a first stage in the construction of the magnetite-paper device, Fe_3O_4@PDA is disposed on a paper surface under ultrasound treatment to obtain "appropriate deposition". Cellulose paper is mainly composed of a homopolymer of (1-4)-β-glucopyranose linked through acetal bonds and forming long β-1,4-glucan chains. The hydroxyl groups of these chains make the paper hydrophilic with a negative charge. As a result, paper can only adsorb cationic molecules while polydopamine molecules at neutral pH are negatively charged due to deprotonation of the phenolic group.[42] The incompatibility between Fe_3O_4@PDA dispersion and cellulose paper is unfavorable for the adherence of these two materials and the core–shell layer on paper is non-homogenous and hence, also the antibodies deposition (see ESI, Fig. S8†).

Summarizing, according to Raman experiments the Fe_3O_4@W1-PDA-AntiIgM was the system with suitable homogeneity of AntiIgM antibodies covering the surface.

"Magnetic Paper – Based ELISA" performance

The described commercial standard UMELISA Dengue IgM Plus assay was slightly modified by using Fe_3O_4 nanoparticles

deposited on papers as solid phase instead of using microwells. The effectiveness of a blocking step should be taken into account to achieve suitable results. In this sense, the different magnetite-PDA coated papers and pristine papers were treated with traditional blockers and, after a washing step, streptavidin-alkaline phosphatase (S-AP) was added. In addition, the systems without blockers were treated with S-AP to confirm whether protein adsorption had taken place. The pristine papers with S-AP have negligible fluorescence intensities (see ESI, Fig. S9†). This result indicates poor protein adsorption (even at 4 hours) on cellulose, confirming the necessary presence of magnetite nanoparticles as a requirement for protein capture, allowing a suitable ELISA performance. Also, magnetite-PDA coated ss903 papers exhibited higher protein conjugation than paper type W1, confirming the highest loading protein capability. Finally, milk solution was the most efficient blocker used to diminish unspecific protein adsorption on magnetite nanoparticles and cellulose channels, which allows low fluorescence background.

For the "Magnetic Paper – Based ELISA" the higher the amount of conjugated IgM-dengue, with a suitable spatial conformation for dengue antigen recognition, the higher the fluorescence intensity. Therefore, high fluorescence intensity will correspond to a better efficacy for the solid support (NPs or magnetite-papers systems) for IgM-dengue capture.

As a first step, a titration was performed in order to estimate the effective amount of Fe_3O_4@PDA-AntiIgM in suspension for capturing as many IgM-dengue antibodies (see ESI, Fig. S10†). For this purpose, different amounts (in the range from 0.1 mg to 1 mg) of magnetite core further functionalized with PDA were tested in ELISA micro-well containers. A plateau for IgM-dengue capture in the magnetic-ELISA performance was obtained for 1 mg of magnetite reaching the saturation response. However, this amount is handled in micro-well plates with magnets, which is very awkward, provoking handling mass losses and undesired analytical effects. In this sense, a pragmatic and effortless system with good analytical performance by using magnetic paper-based ELISA principles is proposed. Therefore, a small amount of particles can be deposited on paper, and working with it without loss from operator handling, thus improving analytical response.

Fig. 4 shows fluorescence emission intensities for the different paper-based systems. In addition, for a comprehensive analysis and according to the magnetite composition of different coated papers, the fluorescence intensities for Fe_3O_4@PDA nanoparticles in suspension with magnetite core amounts of 0.1 mg and 0.3 mg as reference were determined. At this point, pristine ss903 and W1 papers were not taken into account as a ELISA solid support due to their unfeasibility for protein retention, as was confirmed in the blocking study.

As observed in Fig. 4, the system Fe_3O_4@ss903-PDA shows the highest fluorescence intensity followed by Fe_3O_4@W1-PDA composite. Additionally, for both cases, higher intensities were obtained than nanoparticles in suspension by using similar magnetite amounts (0.3 and 0.1 mg, according to the case). Many factors could be influencing the results. First, Fe_3O_4@ss903-PDA presents a higher amount of coupled

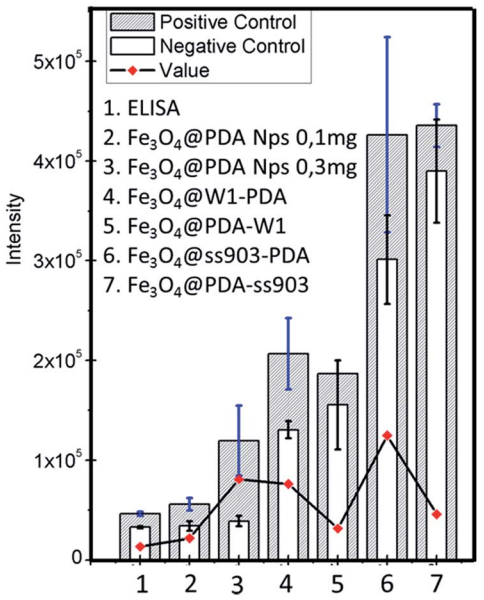

Fig. 4 UMELISA DENGUE IgM PLUS assays for different solid supports: (1) traditional ELISA micro-wells, (2 and 3) Fe_3O_4@PDA with 0.1 and 0.3 mg respectively, of magnetite core, (4) Fe_3O_4@W1-PDA, (5) Fe_3O_4@PDA-W1, (6) Fe_3O_4@ss903-PDA, and (7) Fe_3O_4@PDA-ss903. The positive control is IgM-dengue and the negative control BSA solution. The amount of IgM-dengue antibodies used as positive control was 0.09 mg, which corresponds with the cut-off value established in the commercial traditional ELISA. The red spots were obtained by subtracting the positive control spectra to the negative control spectra (3 replicates were measured for each case).

AntiIgM and IgM-dengue with lower magnetite nanoparticles quantity, which could lead to suitable antibodies capability.

However, according to the SDS-PAGE Raman experiments and blocking study, the Fe_3O_4@ss903-PDA system exhibited noticeable unspecific interactions with proteins and non-homogenous disposition of the antibodies on magnetite-paper surface.

These observations explain the non-negligible background (particularly noticeable for coated paper ss903), the highest standard deviation value, and consequently low reproducibility. On the contrary, the analogue system using paper type W1, presents a slight fluorescence background with appropriate standard deviation due to paper features and homogenous antibodies covering.

In the cases of Fe_3O_4@PDA-W1 and Fe_3O_4@PDA-ss903, these composites display higher background and hence lower final fluorescence intensities even compared with Fe_3O_4@PDA in suspension. As was already explained, Fe_3O_4@PDA-paper-AntiIgM-IgM presented non-homogeneous nanoparticles and antibodies covering on papers, which dramatically attend the magnetic paper-based ELISA performance.

In order to demonstrate the analytical improvement of Fe_3O_4@W1-PDA as a new platform for dengue recognition, a sandwich immunoassay for measuring different IgM-dengue concentrations was performed. Fig. 5b–d shows the corresponding calibration curves. Good linearity of the calibration curves was obtained for Fe_3O_4@PDA nanoparticles in

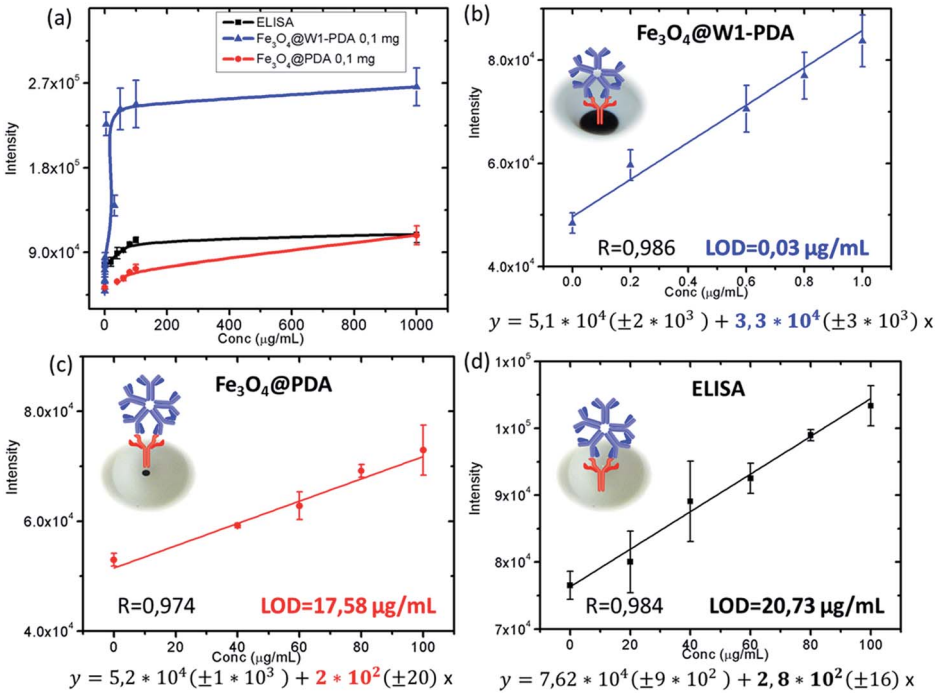

Fig. 5 (a) Analytical response and calibration curves for (b) Fe_3O_4@W1-PDA, (c) Fe_3O_4@PDA 0.1 mg, and (d) standard ELISA.

suspension (0.1 mg) (Fig. 5c) and standard ELISA (Fig. 5d) in the concentration range from 20 to 100 μg mL^{-1} with almost equal sensitivities (interpreted as the calibration curve slope). However, Fe_3O_4@W1-PDA (Fig. 5b) shows good linearity of the calibration curve in a range of 0.03 to 1 μg mL^{-1} with 100 times more sensitivity and 700 times lower limit of detection (S/N = 3) than traditional ELISA or using magnetic beads without depositing on paper to detect IgM-dengue antibodies.

The analytical performance of Fe_3O_4@W1-PDA compared with Fe_3O_4@PDA nanoparticles in suspension and traditional ELISA is in complete correspondence with the amount of coupled AntiIgM. The AntiIgM amount for 5 mm of Fe_3O_4@W1-PDA paper (0.1 mg of magnetic core) was 2.3 μg; for Fe_3O_4@PDA Nps (0.1 mg of magnetic core) it was 1.8 μg; and for the ELISA method it was under Bradford limit of detection (see ESI Table S2†).

This result is in agreement with the higher surface area of Fe_3O_4@paper-PDA than pristine paper with noticeable loading capacity due to its porous structure and hydrophilic channels.

To validate the analytical accuracy of the developed magnetic paper – based ELISA method by using Fe_3O_4@W1-PDA as solid support for detection of real samples, healthy human serum samples were spiked with different concentrations of control IgM-dengue. As Table 2 shows, the recoveries of the spiked human IgM-dengue ranged from 95% to 102%. The satisfactory recoveries of very low concentrations of IgM-dengue indicate that such a method has good specificity and is applicable to the quantification of IgM-dengue antibodies in complex biological samples. Also, it is very important to remark that the LOD of magnetic paper – based ELISA method in real samples, 0.04 μg mL^{-1}, is 500 times lower than the threshold concentration for clinical IgM-dengue diagnosis with traditional ELISA (20 μg mL^{-1}) (see ESI, Fig. S11†).

Approximately, more than 50 commercial MAC-ELISA kits are available for IgM-dengue detection. In almost all cases the analytical parameters (sensitivity, specificity, false positives, and cross reactivity) are based on statistical studies of a population of a huge amount of patient serum samples[43–47] and not in terms of traditional calibration curves, linear range, sensitivity interpreted as the slope, limit of detection, serum dilutions, accuracy from recovery data, and cross-reactivity by using standard antigens.

In addition, despite the fact that there are enormous amounts of commercial MAC-ELISA kits, there is a lack of reports about nanomaterial-based immunoassays and biosensors for IgM detection. Thus, a comparative study between the magnetic-paper-based ELISA reported in this study with other methods mentioned above could be disappointing. Table 3 shows some limit of detections (LODs) of immunoassays and biosensors designed for IgM antibodies detection. Generally, the system proposed in this work presented a lower LOD with specific IgM-dengue detection than the others. It is important to point out that during the early stages of dengue infection, virus

Table 2 Detection of IgM-dengue spiked in human serum samples by magnetic paper – based ELISA method with Fe_3O_4@W1-PDA (n = 3)

Samples	Added IgM-dengue (μg mL^{-1})	Found IgM-dengue (μg mL^{-1})	Recovery (%)
1	0.4	0.38 ± 0.02	95 ± 7
2	0.6	0.59 ± 0.03	99 ± 7
3	0.8	0.82 ± 0.05	102 ± 8

Table 3 Comparison of the analytical performance of some designs for IgM detection

Antibodies	Limit of detection (LOD)	Design
IgM non specific	150 ng mL^{-1} (in buffer)	Surface plasmon resonance (SPR) sensor on Fe_3O_4–AuNR substrate[50]
IgM-dengue	10 times lower than the chemiluminescent MAC-ELISA and 100 times lower than the colorimetric MAC-ELISA. Dilution 10^6 of strong positive serum	Chemiluminescent optical fiber immunosensor (OFIS)[51]
IgM non specific	0.1 ng mL^{-1} (in buffer)	Multiarray optical nanochip based on (LSPR)-bioanalysis method for screening bimolecular interactions[52]
IgM non specific	70 ng (in buffer)	Magnetic solid phase enzyme-immunoassay[53]
IgM-dengue	Dilution 10–100% of strong positive control serum	SPR direct immunoassay by increasing in resonance angle, using gold sensor chip[54]
IgM-dengue	40 ng mL^{-1} (in serum) 0.8 ng (in serum) dilution 1 : 10 000 of positive control. 700 times lower than fluorescent MAC-ELISA	Magnetic paper – based ELISA (this work)

isolation, and nucleic acid or dengue NS1 antigen detection are the leading methodologies for diagnosis.[48] Nevertheless, considering the possible massive amount of infected patients, commercial MAC-ELISAs is the inexpensive chosen method for IgM-dengue antibodies diagnosis in a first-time infection, five or more days after the onset of illness.[49]

However, at this time the infection could be rapidly spreading in a population area triggering hazardous epidemiologic implications. In this sense, taking in account the analytical performance of the developed method in this work, it has potential application for IgM-dengue diagnosis during earlier stages of the disease, thus minimizing infection implications.

However, all reported MAC-ELISA for IgM-dengue detection, including the traditional protocol used in this work, could present inherent false-positive results due to cross-reactivity with other flaviviruses such as Malaria, Leptospirosis, West Nile virus, Zika, Chikungunya, and others.[48]

Nevertheless, just cross-reacting studies with co-circulating flavivirus antibodies could confirm if the proposed application could be or not be possible. Also, this mainly depends on the specificity of the particular commercial MAC-ELISA supported on magnetic paper. IgM tests can be useful for surveillance and support diagnosis of dengue infection in conjunction with clinical symptoms, a patient's past medical history, recent travel history, vaccination record, other epidemiologic information, and combining laboratory confirmatory tests.

Summarizing, Fe_3O_4@W1-PDA as new solid support for IgM-dengue antibodies detection provided a system with improved analytical response (sensibility, limit of detection, accuracy, and background), low cost, easy manufacturing, and effortless and easy handling.

The requirements for using magnetite-PDA coated paper for a suitable magnetic-ELISA performance are endorsed for several key aspects: (i) the negligible effectiveness of pristine W1 and ss903 papers for an effective protein coupling; (ii) the high contact surface area of magnetite nanoparticles increasing the amount of coupled antibodies; (iii) the proven efficacy of polydopamine as an antibodies linker without losing their recognition capabilities or the need for using coupling agents; (iv) the washing automated protocols through the use of magnets allowing multiple samples operation; (v) the use of small amounts of magnetite nanoparticles on a paper surface without loss by operator handling; and (vi) the microfiber network morphology of cellulose paper leading to protein retention.

Conclusions

Fe_3O_4 nanoparticles were synthesized by coprecipitation of Fe^{2+}/Fe^{3+} ions in alkali media and then capped with polydopamine film through the spontaneous self-polymerization of dopamine. Two ways for coating paper with Fe_3O_4@PDA and functionalized with AntiIgM were considered. Fe_3O_4@ss903-PDA presented a high amount of coupled AntiIgM and IgM-dengue with a lower magnetite nanoparticles amount and also the highest standard deviation value and consequently low reproducibility were observed. Fe_3O_4@W1-PDA exhibited suitable analytical response with slight fluorescence background and appropriate standard deviation due to paper features and homogenous antibodies covering. Fe_3O_4@PDA-W1 and Fe_3O_4@ss903-PDA display higher background and lower final fluorescence intensities due to non-homogeneous Fe_3O_4@PDA nanoparticles and antibodies covered papers. According to magnetic-paper based ELISA performance, the system Fe_3O_4@W1-PDA is two orders more sensitive with a 700 times in PBS and 500 times in serum lower limit of detection than traditional ELISA for IgM-dengue detection.

Acknowledgements

The authors acknowledge the Center of Protein Studies, Faculty of Biology, University of Havana, Cuba; the Immunoassay Center, Cuba; the Center of Molecular Immunology, Cuba and the Center for Applied Science and Advanced Technology of IPN, Legaria Unit, Mexico for access to their experimental facilities. This study was partially supported by the CONACyT (Mexico) Projects 2013-05-231461, and CB-2014-01-235840. G. A.

O. thanks the support provided by SIP-IPN through an innovation project for student.

References

1 E. Engvall and P. Perlmann, *J. Immunol.*, 1972, **109**, 129–135.
2 A. Lin, L. Nguyen, T. Lee, L. M. Clotilde, J. A. Kase, I. Son, J. M. Carter and C. R. Lauzon, *J. Microbiol. Methods*, 2011, **87**, 105–110.
3 J. Liu, G. Kibiki, V. Maro, A. Maro, H. Kumburu, N. Swai, M. Taniuchi, J. Gratz, D. Toney, G. Kang and E. Houpt, *J. Clin. Virol.*, 2011, **50**, 308–313.
4 D. C. Andrade, I. C. Borges, H. Laitinen, N. Ekström, P. V. Adrian, A. Meinke, A. Barral, C. M. Nascimento-Carvalho and H. Käyhty, *J. Immunol. Methods*, 2014, **405**, 130–143.
5 K. E. Sapsford, W. Russ-Algar, L. Berti, K. Boeneman-Gemmill, B. J. Casey, E. Oh, M. H. Stewart and I. L. Medintz, *Chem. Rev.*, 2013, **113**, 1904–2074.
6 V. Kourilov and M. Steinitz, *Anal. Biochem.*, 2002, **311**, 166–170.
7 F. Li, R. Zhou, K. Zhao, H. Chen and Y. Hu, *Talanta*, 2011, **87**, 302–306.
8 A. D. Stefano, G. Volpe, G. Adornetto, S. Bernardini, M. Nuccetelli, G. Gallucci, L. D. Ruvo and D. Moscone, *Electroanalysis*, 2014, **26**, 1382–1389.
9 S. Jeong, J. Park, D. Pathania, C. M. Castro, R. Weissleder and H. Lee, *ACS Nano*, 2016, **10**, 1802–1809.
10 C. Hu, I. Zeimpekis, K. Sun, S. Anderson, P. Ashburn and H. Morgan, *Anal. Chem.*, 2016, **88**, 4872–4878.
11 T. S. Safaei, R. M. Mohamadi, E. H. Sargent and S. O. Kelley, *ACS Appl. Mater. Interfaces*, 2015, **7**, 14165–14169.
12 J. Liu, L. Zhang, Y. Wang, Y. Zheng and S. Sun, *Measurement*, 2014, **47**, 200–206.
13 J. G. Bruno, A. M. Richarte and T. Phillips, *Microchem. J.*, 2014, **115**, 32–38.
14 L. Wei, J. Wei, D. Shuang and W. Lei, *Anal. Chem.*, 2016, **88**, 1578–1584.
15 B. A. Otieno, C. E. Krause, A. Latus, B. V. Chikkaveeraiah, R. C. Faria and J. F. Rusling, *Biosens. Bioelectron.*, 2014, **53**, 268–274.
16 K. Kriz, F. Ibraimi, M. Lu, L. O. Hansson and D. Kriz, *Anal. Chem.*, 2005, **77**, 5920–5924.
17 A. Ambrosi, M. T. Castañeda, A. J. Killard, M. R. Smyth, S. Alegret and A. Merkoçi, *Anal. Chem.*, 2007, **79**, 5232–5240.
18 L. Hung, J. Chang, Y. Tsai, C. Huang, C. Chang, C. Yeh and G. Lee, *J. Nanomed. Nanotechnol.*, 2014, **10**, 819–829.
19 H. Y. Tsaia, J. R. Chan, Y. C. Li, F. C. Cheng and C. Bor Fuhb, *Biosens. Bioelectron.*, 2010, **25**, 2701–2705.
20 B. Tian, T. Zardan Gomez de la Torre, M. Donolato, M. F. Hansen, P. Svedlindh and M. Stromberg, *Anal. Methods*, 2016, **8**, 5009–5016.
21 S.-L. Ho, D. Xu, S. W. Man and H.-W. Li, *Chem. Sci.*, 2016, **7**, 2695–2700.
22 G. Fu, S. T. Sanjay and X. Li, *Analyst*, 2016, **141**, 3883–3889.
23 G. Suqin and X. Yunsheng, *Chem. Commun.*, 2016, **52**, 9660–9663.
24 M. E. Cortina, L. J. Melli, M. Roberti, M. Mass, G. Longinotti, S. Tropea, P. Lloret, D. A. R. Serantes, F. Salomón, M. Lloret, A. J. Caillava, S. Restuccia, J. Altcheh, C. A. Buscaglia, L. Malatto, J. E. Ugalde, L. Fraigi, C. Moina, G. Ybarra, A. E. Ciocchini and D. J. Comerci, *Biosens. Bioelectron.*, 2016, **80**, 24–33.
25 Y. L. Chemla, H. L. Grossman, Y. Poon, R. McDermott, R. Stevens, M. D. Alper and J. Clarke, *Proc. Natl. Acad. Sci. U. S. A.*, 2000, **97**, 14268.
26 D. Baselt, G. U. Lee, M. Natesan, S. W. Metzger, P. E. Sheehan and R. J. Colton, *Biosens. Bioelectron.*, 1998, **13**, 731.
27 J. F. T. Aytur, M. Anwar, B. Boser, E. Harris and P. R. Beatty, *J. Immunol. Methods*, 2006, **314**, 21–29.
28 M. Muluneh and D. Issadore, *Adv. Drug Delivery Rev.*, 2014, **66**, 101–109.
29 S. D. Soelberg, R. C. Stevens, A. P. Limaye and C. E. Furlong, *Anal. Chem.*, 2009, **81**, 2357–2363.
30 V. Singh, C. Rodenbaugh and S. Krishnan, *ACS Sens.*, 2016, **1**, 437–443.
31 P. Douglas, R. J. Stokes, D. Graham and W. E. Smith, *Analyst*, 2008, **133**, 791–796.
32 C.-M. Cheng, A. W. Martinez, J. Gong, C. R. Mace, S. T. Phillips, E. Carrilho, K. A. Mirica and G. M. Whitesides, *Angew. Chem., Int. Ed.*, 2010, **49**, 4771–4774.
33 C. K. Tang, A. Vazea and J. F. Rusling, *Anal. Methods*, 2014, **6**, 8878–8881.
34 A. C. Glavan, D. C. Christodouleas, B. Mosadegh, H. D. Yu, B. S. Smith, J. Lessing, M. T. Fernández-Abedul and G. M. Whitesides, *Anal. Chem.*, 2014, **86**, 11999–12007.
35 A. W. Martinez, *Bioanalysis*, 2011, **3**, 2589–2592.
36 R. L. Rebodos and P. J. Vikesland, *Langmuir*, 2010, **26**, 16745–16753.
37 E. Faure, C. Falentin-Daudré, C. Jérôme, J. Lyskawa, D. Fournier, P. Woisel and C. Detrembleur, *Prog. Polym. Sci.*, 2013, **38**, 236–270.
38 M. Martín, A. G. Orive, P. Lorenzo-Luis, A. H. Creus, J. L. González-Mora and P. Salazar, *ChemPhysChem*, 2014, **15**, 3742–3752.
39 M. Martin, P. Salazar, R. Villalonga, S. Campuzano, J. M. Pingarron and J. L. Gonzalez-Moraa, *J. Mater. Chem. B*, 2014, **2**, 739–746.
40 M. Martín, P. Salazar, C. Jiménez, M. Lecuona, M. J. Ramos, J. Ode, J. Alcoba, R. Roche, R. Villalonga, S. Campuzano, J. M. Pingarrón and J. L. González-Mora, *Anal. Chim. Acta*, 2015, **5**, 51–58.
41 G. A. Ortega, J. C. Zuaznabar-Gardona, O. Morales-Tarré and E. Reguera, *RSC Adv.*, 2016, **6**, 98457–98465.
42 Q. Liu, B. Yu, W. Ye and F. Zhou, *Macromol. Biosci.*, 2011, **11**, 1227–1234.
43 E. A. Hunsperger, S. Yoksan, P. Buchy, V. C. Nguyen, S. D. Sekaran, D. A. Enria, J. L. Pelegrino, S. Vázquez, H. Artsob, M. Drebot, D. J. Gubler, S. B. Halstead, M. G. Guzmán, H. S. Margolis, C.-M. Nathanson, N. R. R. Lic, K. E. Bessoff, S. Kliks and R. W. Peeling, *Emerging Infect. Dis.*, 2009, **15**, 436–440.

44 M. G. Guzman, S. B. Halstead, H. Artsob, P. Buchy, J. Farrar, D. J. Gubler, E. Hunsperger, A. Kroeger, H. S. Margolis, E. Martínez, M. B. Nathan, J. L. Pelegrino, C. Simmons, S. Yoksan and R. W. Peeling, *Nat. Rev. Microbiol.*, 2010, S7–S16.

45 S. D. Blacksell, R. G. Jarman, R. V. Gibbons, A. Tanganuchitcharnchai, J. Mammen, P. Mammen, A. Nisalak, S. Kalayanarooj, M. S. Bailey, R. Premaratna, H. J. d. Silva, N. P. J. Day and D. G. Lalloog, *Clin. Vaccine Immunol.*, 2012, **19**, 804–810.

46 R. J. Welch, G.-J. J. Chang and C. M. Litwin, *J. Virol. Methods*, 2014, **195**, 247–249.

47 O. Parkash and R. H. Shueb, *Viruses*, 2015, **7**, 5410–5427.

48 N. T. Darwish, Y. B. Alias and S. M. Khor, *TrAC, Trends Anal. Chem.*, 2015, **67**, 45–55.

49 *Dengue guidelines for diagnostic, treatment, prevention and control*, World Health Organization (WHO) and the Special Programme for Research and Training in Tropical Diseases (TDR), Geneva, 2nd edn, 2009.

50 H. Zhang, Y. Sun, J. Wang, J. Zhang, H. Zhang, H. Zhou and D. Song, *Biosens. Bioelectron.*, 2012, **34**, 137–143.

51 D. Atias, Y. Liebes, V. Chalifa-Caspi, L. Bremand, L. Lobel, R. S. Marks and P. Dussart, *Sens. Actuators, B*, 2009, **140**, 206–215.

52 T. Endo, K. Kerman, N. Nagatani, H. M. Hiepa, D.-K. Kim, Y. Yonezawa, K. Nakano and E. Tamiya, *Anal. Chem.*, 2006, **78**, 6465–6475.

53 J. L. Guesdon and A. Stratis, *Immunochemistry*, 1977, **14**, 443–447.

54 S. Kumbhat, K. Sharma, R. Gehlot, A. Solanki and V. Joshi, *J. Pharm. Biomed. Sci.*, 2010, **52**, 255–259.

